Xue *et al.*
Chinese Journal of Mechanical Engineering (2021) 34:130
https://doi.org/10.1186/s10033-021-00644-6

Chinese Journal of Mechanical Engineering

ORIGINAL ARTICLE

Open Access

Approach for Obtaining Material Mechanical Properties in Local Region of Structure Based on Accurate Analysis of Micro-indentation Test

He Xue[1*], Jinxuan He[1], Jianlong Zhang[2] and Yuxuan Xue[3]

Abstract

The hot or cold processing would induce the change and the inhomogeneous of the material mechanical properties in the local processing region of the structure, and it is difficult to obtain the specific mechanical properties in these regions by using the traditional material tensile test. To accurately get actual material mechanical properties in the local region of structure, a micro-indentation test system incorporated by an electronic universal material test device has been established. An indenter displacement sensor and a group of special micro-indenter assemblies are established. A numerical indentation inversion analysis method by using ABAQUS software is also proposed in this study. Based on the above test system and analysis platform, an approach to obtaining material mechanical properties in the local region of structures is proposed and established. The ball indentation test is performed and combined with the energy method by using various changed mechanical properties of 316L austenitic stainless steel under different elongations. The investigated results indicate that the material mechanical properties and the micro-indentation morphological changes have evidently relevance. Compared with the tensile test results, the deviations of material mechanical parameters, such as hardness H, the hardening exponent n, the yield strength σ_y, and others are within 5% obtained through the indentation test and the finite element analysis. It provides an effective and convenient method for obtaining the actual material mechanical properties in the local processing region of the structure.

Keywords: Structural integrity assessment, Micro-indentation test, Numerical testing inversion analysis, Local material mechanical property

1 Introduction

Manufacturing mechanical structures process, including welding and other hot or cold processes, has been broadly adopted in the industrial field [1, 2]. It has been reported that the mechanical properties of metal materials would be changed after the cold or hot processing [3, 4]. Because the local area involved in hot and cold processing is easy to occur flaw and failure, it is a key area for structural integrity analysis [5]. And obtaining the specific mechanical properties in these local area of structures in the structural integrity analysis will contribute to the further understanding of manufacturing processing [6, 7].

It is of great practical significance to develop a test and calibration method to obtain the mechanical property parameters and distribution law of inhomogeneous welded joint materials [8]. The indentation test has been widely used as a non-destructive testing method that does not affect the continued service of equipment and is easy to operate [9, 10]. Scholars have done researches on the measurement of mechanical properties by the indentation method [11, 12]. As early as 1961, Stillwell et al. [13] proposed determining the mechanical properties by using the elastic recovery generated through the indenter to press into the material. Bulychev et al. [14]

*Correspondence: xuehe@xust.edu.cn
[1] School of Mechanical Engineering, Xi'an University of Science and Technology, Xi'an 710054, China
Full list of author information is available at the end of the article

measured the contact area through the unloaded part of the load-displacement curve, which laid the foundation for the later indentation hardness test. Haggag et al. [15] studied the representative strain of the indentation plastic zone and obtained a series of relations, which played an essential role in the subsequent research on the indentation method to characterize the stress and strain. Das et al. [16] studied the constitutive relationship and strength properties of two high-strength, low-alloy steels under different pre-strains using a continuous ball indentation method. Wei et al. [17, 18] used nano-indentation to study the stress-strain relationship of metal thin film materials and carried out detailed characterization of the mechanical properties of different metal materials. Zafar et al. [19] evaluated a method to infer powder flowability by the ball indentation, and the technique can be applied at very low loads using a small sample quantity. Zhang et al. [20, 21] estimated the fracture toughness of Q235B steel by automatic ball indentation test. They obtained the residual stress distribution of different kinds of austenitic stainless steel materials through the analysis of the indentation process. Pamnanil et al. [22] studied the mechanical properties of the welded area with different welding methods in the high-strength and low-alloy steel structure by using the ball indentation test. These researches indicate that it is possible to obtain the material properties by an indentation test.

The complex thermal cycle in the welding will cause significant changes in the microstructure and chemical composition of the material in welded joint, which would also produce a complicated local stress state in a welded joint. To represent the effect of the hot or cold processing of materials, the change of local material mechanical properties is performed by the different degrees of tensile deformation in this paper [23, 24]. After rolling, extrusion, roll forging, heat treatment, and other processes, due to the difference in the preferred orientation and mechanical behavior of crystals, there will be differences in grain state and microstructure properties in different directions within the material, resulting in different mechanical properties, yield behavior, and plastic deformation abilities. The anisotropy produced by material leads to different yield behavior and plastic deformation capacities. We simplified the work hardening of materials in the manufacturing process to different degrees of tensile deformation of materials. When studying the mechanics of austenitic stainless steel under a single variable with different plastic hardening effects, the anisotropy has little on the laws obtained from indentation test results. Therefore, we does not consider the various and complex mechanical effects of anisotropic for the time being in this study, and we still consider the materials are isotropic for research. Thus an approach to obtaining the material mechanical properties combined with the ball indentation test and finite element inversion to characterize the mechanics of 316L austenitic stainless steel is discussed and studied.

2 Theoretical Principle

Under the action of an external force, the metal will undergo rapid and instantaneous elastoplastic deformation [25]. In the elastic deformation stage, there is a linear correlation between stress and strain. There is a power-rate relationship between stress and strain for the subsequent plastic deformation stage, called the Hollomon relationship. Austenitic stainless steel and nickel-based alloys are widely used in structures of the nuclear power plant. The stress-strain relationship of these metal materials meets the stress-strain relationship of linear elastic-power hardening materials, so that it can be expressed by the Hollomon equation.

For the metals with hardening characteristics [26], the stress-strain curve can be defined as:

$$\boldsymbol{\sigma} = \begin{cases} \boldsymbol{E\varepsilon} & (\sigma \le \sigma_y), \\ K\boldsymbol{\varepsilon}^{\boldsymbol{n}} = \boldsymbol{E\varepsilon}_y^{1-\boldsymbol{n}}\boldsymbol{\varepsilon}^{\boldsymbol{n}} & (\sigma \ge \sigma_y), \end{cases} \tag{1}$$

$$\boldsymbol{\varepsilon} = \boldsymbol{\varepsilon}_y + \boldsymbol{\varepsilon}_p, \tag{2}$$

where $\boldsymbol{\sigma}_y$ is initial yield stress; $\boldsymbol{\varepsilon}$ is total strain; $\boldsymbol{\varepsilon}_y$ is initial yield strain; $\boldsymbol{\varepsilon}_p$ is plastic strain; $\boldsymbol{E}$ is Young's modulus; K is strength factor; $\boldsymbol{n}$ is the strain hardening exponent.

When $\boldsymbol{\sigma} > \boldsymbol{\sigma}_y$, the plastic stress $\boldsymbol{\sigma}$ can be expressed by

$$\boldsymbol{\sigma} = \boldsymbol{\sigma}_y\left(1 + \frac{\boldsymbol{E}}{\boldsymbol{\sigma}_y}\boldsymbol{\varepsilon}_p\right)^{\boldsymbol{n}}. \tag{3}$$

The micro-nano indentation test mainly includes two stages of loading and unloading. In the loading phase, the indenter enters the surface of a sample. The area will undergo elastic deformation. As the applied load gradually increases, the area with the most considerable elastic deformation will enter the elastoplastic stage, where plastic deformation occurs [27].

The Oliver-Pharr method is commonly used to obtain the mechanical properties of materials by indentation method [28]. Many studies have shown that the load-depth curve is mainly used to obtain parameters such as hardness and Young's modulus. The mechanical properties of the plastic stage are mainly obtained through the dimensional method. The typical load-depth curve for the indentation test is shown in Figure 1. Taking the spherical indenter for the indentation test, Figure 2 shows a schematic diagram of the indentation profile geometry of the test material.

In Figures 1 and 2, h_{max} is the maximum depth value in the load-depth curve; P_{max} is the maximum load value; S

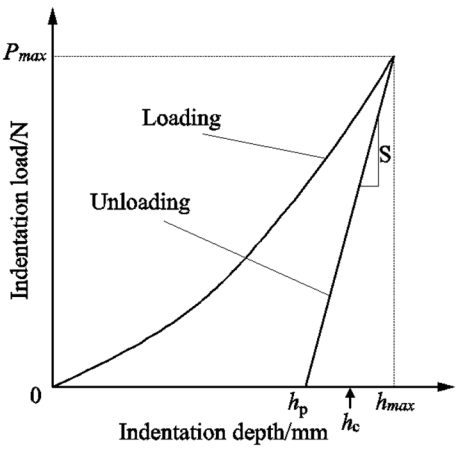

Figure 1 The typical load-depth curve

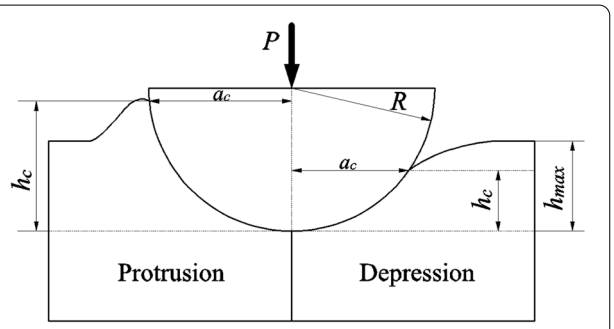

Figure 2 A schematic diagram of indentation profile geometry

is the highest slope value of the unloading curve; h_p is the residual indentation depth; h_c is the contact depth value in the indentation process; a_c is the contact radius in the indentation test, and R is the ball indenter radius.

For a given shape of the indenter, the hardness value of the material can be obtained by

$$\boldsymbol{H} = \frac{P_{\max}}{A}, \tag{4}$$

where A is indentation contact area, and $A=2\pi r h_c$.

For the elastic contact theory, we ignore the influence of direction, size, and border effects of microscopic materials. The geometric size of the gauge length section of the sample is much larger than the maximum indentation depth. The surface of the sample is a geometric plane and is considered to be anisotropic material, such as

$$E_{IT} = \frac{1-\nu^2}{\frac{1}{E_r} - \frac{1-\nu_i^2}{E_i}}, \tag{5}$$

where E_{IT} is the Young's modulus of the sample material; ν is the Poisson's ratio of the sample material; E_i is the Young's modulus of the indenter material; ν_i is the Poisson's ratio of the indenter material. Diamond is usually selected as the indenter material, where $E_i = 1140$ GPa, $\nu = 0.07$.

In the plastic parameter identification, the optimization method is usually used to calculate the plastic mechanical parameters in the indentation process. Through the indentation test simulations of a large number of materials with different parameter combinations, the input parameters and output results are optimized and fitted. The relationship between the press-in measurable parameters and material parameters is established, and the required mechanical parameters are solved. Based on defining characteristic strain, Tabor [29] obtains the following specific form

$$P = 2.8\pi k a_c^2 (0.2\frac{a_c}{R})^{m-2}, \tag{6}$$

where $k = E\varepsilon^{1\text{-}n}$.

Field et al. [30] take the logarithm based on Eq. (6).

$$\log P = \log\left[2.8\pi k c^{\boldsymbol{n}+2}(\frac{0.2}{R})^{\boldsymbol{n}}\right] + m\log a, \tag{7}$$

where $a = \sqrt{2Rh - h^2}$, $m = \boldsymbol{n}+2$, and n can be calculated from the slope of log$P$ and log$a$ curves.

To simplify the relationship between the analysis parameters and the identification parameters, while reducing the sensitivity of test errors, it has become a concern for this type of method. The accuracy and stability of the analysis method and the comparison verification with the uniaxial tensile test results are important to be involved in identifying plastic mechanical properties.

For the ball indenter, Ma et al. [31] established the relationship between $\boldsymbol{\sigma}_y$ and $\boldsymbol{W}_u/\boldsymbol{W}_t$, and then they established the relationship between $\boldsymbol{\sigma}_b$ and $\boldsymbol{W}_u/\boldsymbol{W}_t$. Where $\boldsymbol{W}_u$ is unloading work, and $\boldsymbol{W}_t$ is the total work from loading to complete unloading.

Based on the description of the related literature on the relationship between the work obtained from the load-depth curve and the mechanical properties of the material, the study focuses on the relationship between unloading work and total work to predict material strength performance. The load-depth curve is composed of plastic work and elastic work. The sum of the two is the total indentation work. The schematic diagram of the composition is shown in Figure 3.

The physical quantities involved in the pressing process include material parameters ($\boldsymbol{E}$, ν, $\boldsymbol{\sigma}_y$, $\boldsymbol{n}$), indenter geometric parameters (R), control variables (h, h_{max}). E

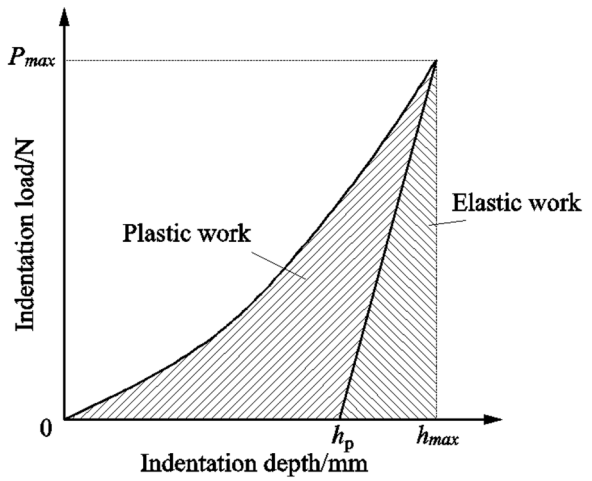

Figure 3 Composition of indentation work

and h are selected as basic quantities, and the indentation loads P, W_u, W_t are expressed by the basic quantities.

In the loading stage, the load P can be expressed as

$$P = f_F(E, \nu, \sigma_y, n, R, h). \tag{8}$$

According to the definition of total indentation work,

$$W_t = \int_0^{h_{\max}} P\mathrm{d}h = \frac{E h_{\max}^3}{3} \prod_1 \left(\frac{\sigma_y}{E}, \nu, n, R\right). \tag{9}$$

The unloading work can be expressed as

$$W_u = \int_{h_p}^{h_{max}} P\mathrm{d}h = E h_{\max}^3 \prod_2 \left(\frac{\sigma_y}{E}, \nu, n, R\right). \tag{10}$$

Through Eqs. (8)–(10), the relationship between unloading work and total indentation work can be obtained as

$$Y = \frac{W_u}{W_t} = \prod_3 \left(\frac{\sigma_y}{E}, \nu, n, R\right). \tag{11}$$

3 Indentation Test

3.1 Sample Preparation

According to the standard GB/T 228- 2002, the 316L plate is rolled into a 2 mm thick steel plate with a coil rolling machine, then cut into 40 mm× 400 mm on a shearing machine. The steel plate online cutting machine is used for slow-moving wire cutting, polishing the burrs, and processing the dowel holes. The geometric

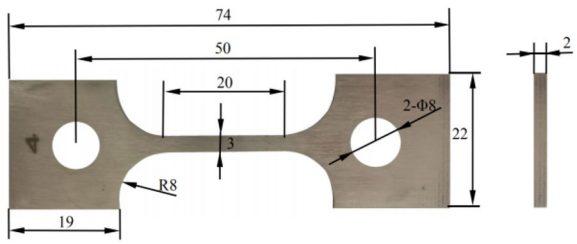

Figure 4 Plate-shaped tensile sample

dimensions of the plate-shaped tensile sample are shown in Figure 4.

The sample was clamped by a U-shaped chuck clamp and fixed on the upper and lower hydraulic chucks of the PLD-500 kN electro-hydraulic servo fatigue tensile testing machine. Then the uniaxial tensile test was carried out. It was setting the room temperature loading rate of the testing machine to 2 mm/min. And the displacement loading method was used in the stretching process. The gauge length section of the sample was pre-stretched by 2 mm, 4 mm and 6 mm, respectively. That the tensile elongation is 10%, 20%, 30%, for simulating the changes of the mechanical properties of materials in hot and cold processing. Sample clamping diagram for the tensile test is shown in Figure 5.

To remove the scratches on the surface and avoid the influence of surface roughness of the sample on the test results, the surface of the samples is evenly sanded with 600#, 1000#, 1500#, 2000# waterproof abrasive paper before the test. The samples need to rotate 90° during

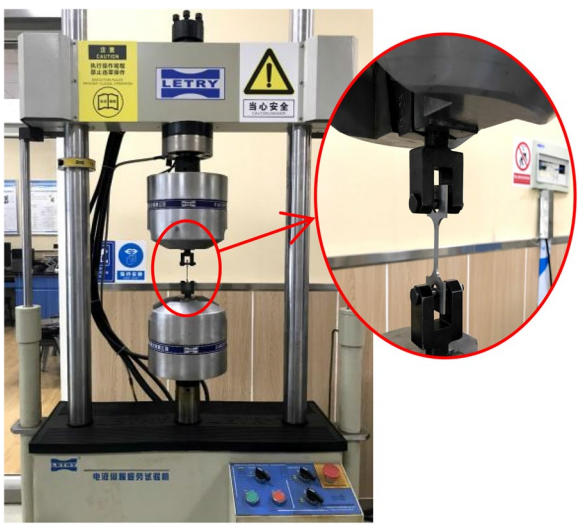

Figure 5 Sample clamping diagram for the tensile test

the sanding process. After the sanding process is completed, the metallographic polishing machine is used to polish the sample. The particle size is 1 W, and the sample scratches are not obvious after polishing to the microscope.

Figure 6(a) shows the engineering stress-strain curves of 316L austenitic stainless steel with different cold working rates obtained through the tensile test. The engineering stress-strain curves obtained are transformed into a true stress-strain curves by Eqs. (12)–(13), as shown in Figure 6(b).

$$\varepsilon_t = \int_{l_0}^{l} \frac{\mathrm{d}l}{l} = \ln\left(\frac{l}{l_0}\right) = \ln\left(1+\varepsilon_e\right), \tag{12}$$

$$\sigma_{\mathrm{t}} = \sigma_e(1+\varepsilon_e). \tag{13}$$

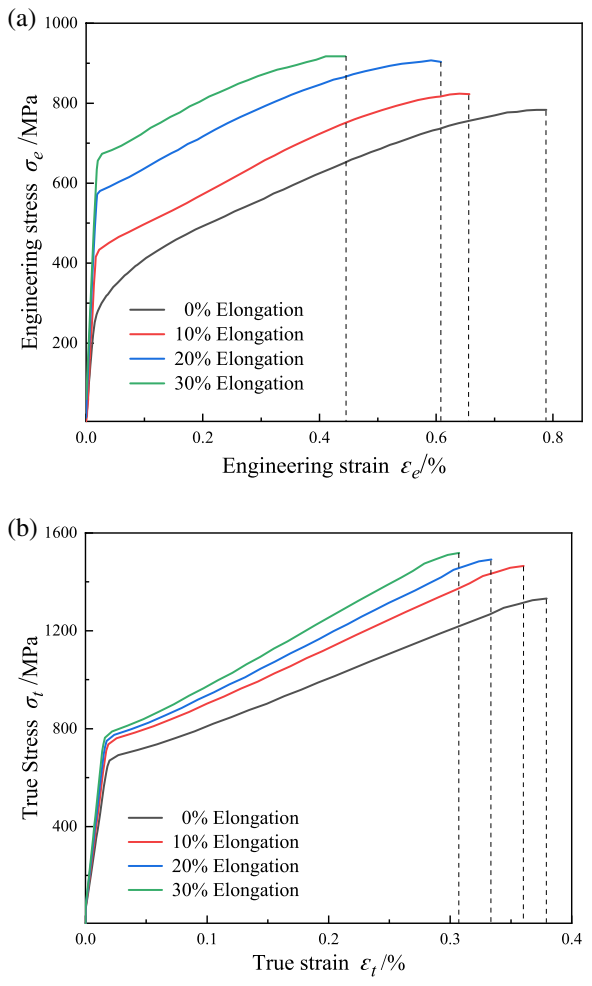

Figure 6 **(a)** Engineering stress-strain curves under different elongations, **(b)** true stress-strain curves under different elongations

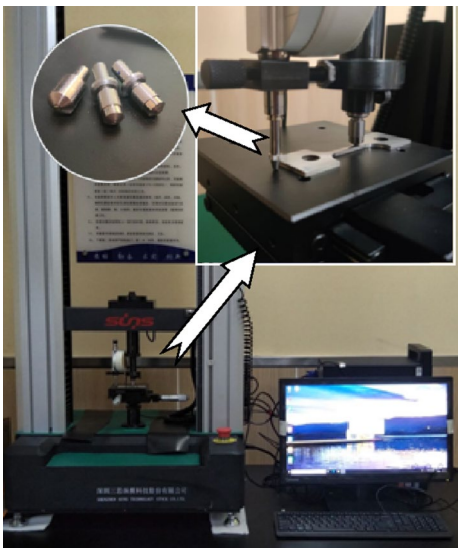

Figure 7 Indentation test system platform

3.2 Parameter Setting of Indentation Test

The indentation test platform has been modified based on the electronic universal material test device. Figure 7 shows the modified indentation test platform.

The loading system of the indentation test platform adopts the electronic drive system of the electronic universal material test device, and the upper chuck is improved to hold different types of indenters. The lower chuck is changed to a sample platform that can be adjusted autonomously in two dimensions. A high-precision displacement sensor is installed on the side of the indenter. The accuracy of the high-precision displacement sensor is 0.5% of the full scale, and the resolution reaches 0.1 μm, and its accuracy satisfies the requirements of the indentation test.

The parameters for setting the indentation test are ball indenter radius, loading and unloading rate, loading and unloading load. The parameter settings of the test platform are as follows.

(1) Ball indenter radius

The ball indenter cannot be greater than one-third of the tested sample. Considering the micro-loss characteristics of indentation testing technology, the cemented carbide spherical indenter with a radius of 0.25 mm is used in the indentation test, and its dimensional accuracy is ±0.001 mm.

(2) Loading and unloading rate

The loading rate is set to 0.5 mm/min, and the unloading rate is set to 0.1 mm/min. The loading process takes

a long time, and more data needs to be collected. During the unloading process, the elastic recovery of the indentation depth is mainly measured. Therefore, the unloading rate is set faster than the loading rate to ensure that the data collected during the entire indentation process is more appropriate.

(3) Loading and unloading load

The loading load is set to 300 N, and the unloading load is set to 3 N. The indentation load with an indentation depth of 0.1–0.2 mm needs to be between 150–300 N. The unloaded load only needs to rebound after the indentation process.

After setting the relevant parameters of the indentation system, the ball indentation test is performed on tested materials with different elongations to obtain the indentation response results.

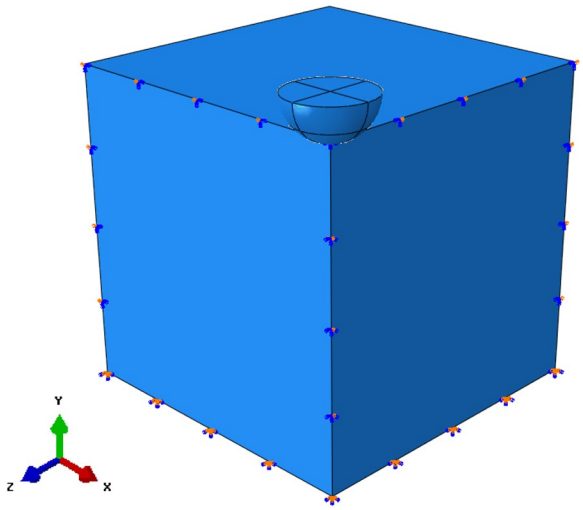

Figure 8 The boundary condition constraints

4 Finite Element Model

The finite element analysis software ABAQUS is used for the indentation simulation test in this paper. The indentation process is entirely symmetric. To facilitate the calculation and ensure the validity of the calculation results, a quarter of the three-dimensional model is established.

In the finite element inversion, the radius of the indenter, the thickness of the tested sample, and the setting of related test parameters are all corresponding to the indentation test.

The elastoplastic deformation parameters of materials with different elongations are obtained from calculating the uniaxial tensile test parameters, and the real stress-strain values are used as the material parameters of the model. For the setting of the material parameters of the indenter, Young's modulus is set to 1×1031 GPa, and the Poisson's ratio is set to 0.3. In the indentation process, the indenter is set to a rigid body.

The indentation finite element model is solved by static force, and the convergence criterion is set to the displacement criterion. The indentation process is controlled by displacement control. In the STEP module of ABAQUS, we set the maximum number of increments as 1000, and the initial increment size is set to 0.001. The loading displacement in the loading analysis step is set to 0.2 mm, the unloading displacement in the unloading analysis step is 0 mm. The bottom of the tested sample is set in Y direction, and the indenter is set to only move in Y direction. The boundary condition constraints are shown in Figure 8.

The quality and quantity of meshes in finite element calculations are critical to the results of analysis. The quality of the grid directly affects the accuracy of the simulation calculation. A reasonable division of the grid can effectively improve the computational efficiency of the finite element model. In this model, the size of the grid is a three-dimensional element grid (CPS4R), and the total number of division units is 44910. The meshes of the contact part of the sample with the indenter need to be refined. The mesh refinement model is shown in Figure 9.

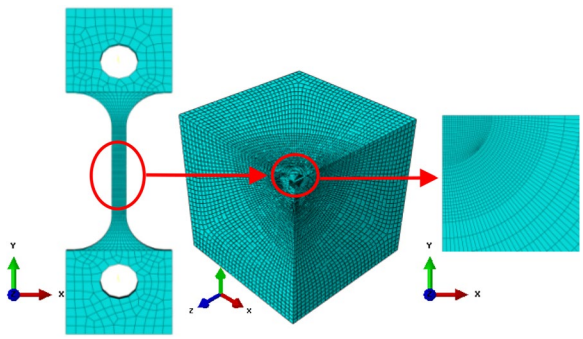

Figure 9 The mesh refinement model

The analysis steps in the finite element inversion are the preloading process, pressing-in process, and unloading process. Setting the preloading step mainly requires the indenter to contact the sample to ensure the accuracy during the indentation process. The press-in step is set to displacement control. Setting the unloading step is mainly to calculate the mechanical properties of the material in the elastic phase. In the contact analysis, the friction coefficient between the indenter and the sample is set to 0.3.

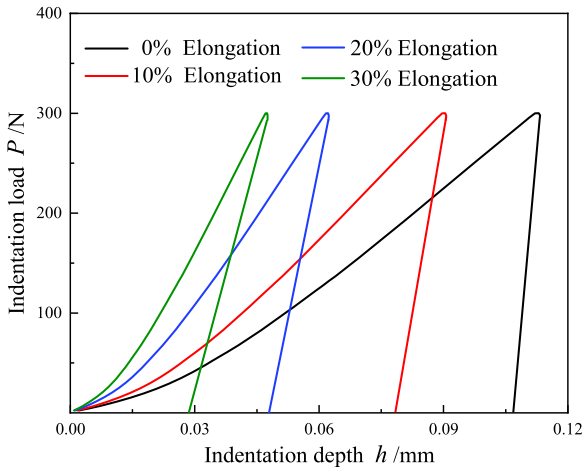

Figure 10 The load-depth curves obtained by indentation test under different elongations

5 Results and Discussions

5.1 Indentation Test Results

The load-depth curves obtained by the indentation test of austenitic stainless steel with no pre-deformation, 10%, 20%, 30% elongation under the indentation load of 0–300 N are shown in Figure 10.

It can be seen from Figure 10 that the loading and unloading trends of the curves are roughly the same. The slope of the curves in the loading phase gradually increase with the increase of the pre-deformation degree. During the unloading stage, the load value per unit area also gradually increases.

After the pre-deformation of the austenitic stainless steel material, the load-depth curves are clearly shifted to the left, indicating that the material becomes harder after pre-deformation, resulting in a smaller indentation response and a smaller residual indentation depth value.

The changes of residual indentation morphology of materials with different elongations observed by the metallurgical microscope after the indentation test are shown in Figure 11.

Comparing the indentation morphology of materials with different elongations in Figure 11, we can see that the plastic deformation increases with the pre-deformation condition, the plastic performance and the indentation response decrease, so that the indentation depth and indentation area are reduced.

When the material is not stretched, the plastic property of the material is strong, and the ability to resist indentation deformation is weak. The indentation area is 0.229 mm^2, the residual indentation depth is 0.117 mm. With the gradual increase of pre-deformation, the materials are affected by work hardening, the indentation area and the indentation depth in indentation tests are reduced. When the elongation is 30%, the indentation area is 0.118 mm^2, and the indentation depth is 0.028 mm.

According to the parameters of load-depth curve and indentation profile information, the hardness values of 316 austenitic stainless steel under different elongations are shown in Figure 12. It can be seen that the hardness of material gradually increases with the increase of elongation.

As the degree of pre-deformation gradually increases, the indentation hardness of the material also increases.

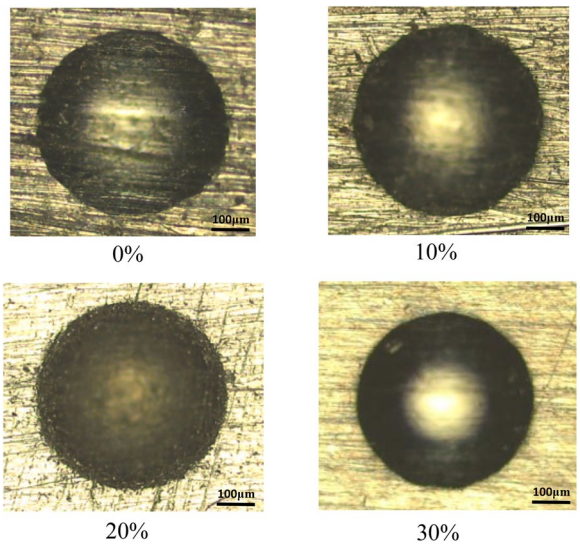

Figure 11 Comparison of indentation morphology with different elongations

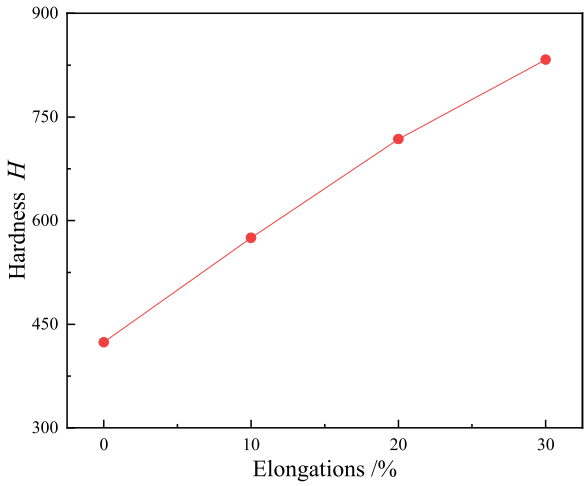

Figure 12 Changing law of hardness under different elongations

Table 1 Load-depth curve parameters of austenitic stainless steel and mechanical parameters with different elongations

Elongation (%)	Unloading work W_u	Total work W_t	Yield strength σ_y(MPa)	Tensile strength σ_b(MPa)	Ratio Y
0	1.52	37.88	350	1331	0.040
10	2.61	50.57	474	1362	0.052
20	4.13	62.93	596	1401	0.066
30	5.46	73.47	685	1452	0.074

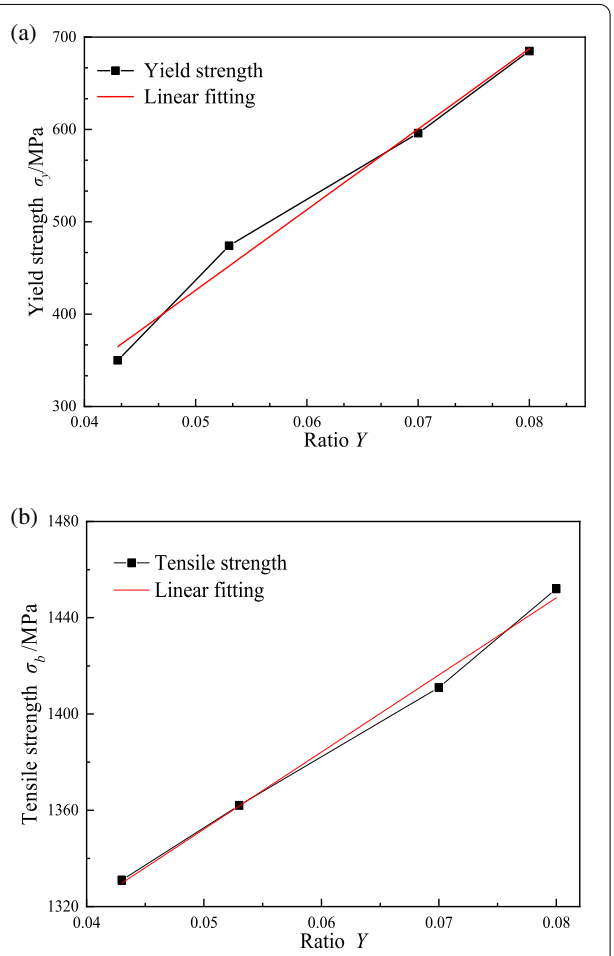

Figure 13 **(a)** Fitting curve of yield strength and ratio *Y*, **(b)** fitting curve of tensile strength and ratio *Y*

When the material is not pre-deformed, the indentation hardness is 424 MPa; when the elongation is 30%, the indentation hardness reaches 833 MPa.

The plastic mechanical parameters of austenitic stainless steel obtained by the indentation method mainly rely on the load-depth curve to calculate the yield strength, yield strain, and hardening exponent.

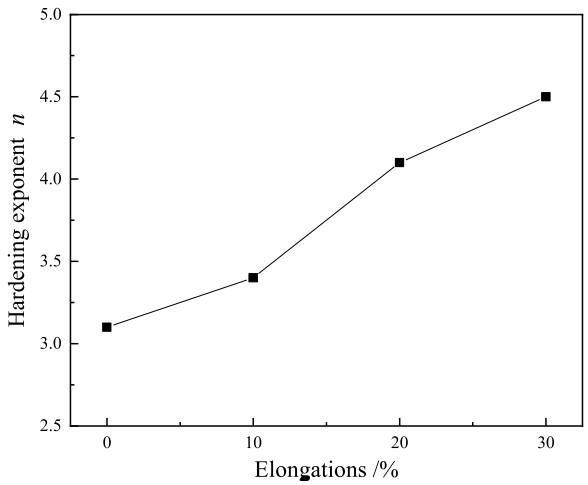

Figure 14 Changing law of hardening exponent under different elongations

For the calculation of yield strength, the area of the curve is used to estimate the energy in the indentation process, and then the strength value is calculated by the obtained energy. The hardening exponent is calculated by the self-similarity theory and the logarithmic slope between the load and the residual indentation area in the load-depth curve. The calculated unloading work, total indentation work, ratio, and yield strength are shown in Table 1.

The yield strength and tensile strength values in Table 1 are fitted linearly to the ratio *Y*, respectively. The fitted curves are shown in Figure 13(a) and (b). The correlation coefficients are $R^2 = 0.998$ and $R^2 = 0.999$, respectively. The linear relations about Eq. (14) and Eq. (15) are obtained as

$$\sigma_y = 9682.38Y - 35.32647, \tag{14}$$

$$\sigma_b = 3632.4Y + 1180.8\,. \tag{15}$$

The hardening exponent values of materials with different elongations are shown in Figure 14. It can be seen

that as the pre-deformation degree of austenitic stainless steel increases, the hardening exponent also increases.

In addition, there is a linear increase relationship between the hardening exponent and the elongations. When the sample is not pre-deformed, the hardening exponent is 3.4. When the elongation is 30%, the hardening exponent reaches 4.5. After the cold working process, the work hardening occurs inside the material, which leads to an increase in the plastic property of the material, so that the hardening exponent of the material also increases.

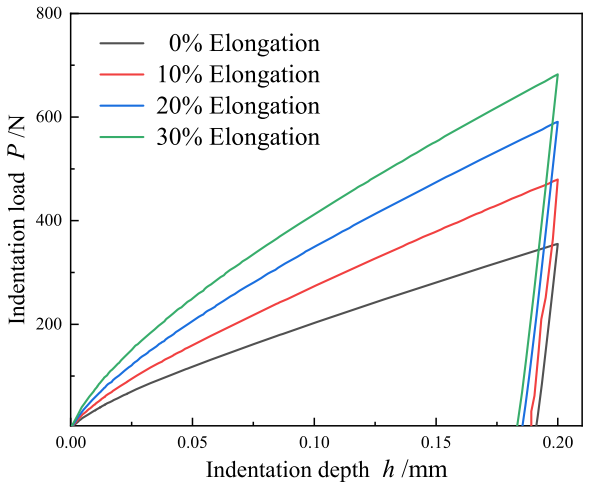

Figure 15 The load-depth curves obtained by finite element reversion under different elongations

5.2 Finite Element Inversion Analysis Results

Figure 15 shows the load-depth curves of 316L austenitic stainless steel under four different elongations through indentation simulation.

It can be seen that the indentation simulation process of materials with different elongations is roughly the same. The loading curve during the pressing process shows a nonlinear trend. As the elongation increases, the required indentation force gradually increases.

In addition, the unloading displacements of the four unloading curves have obvious differences. Pre-deformation has a certain effect on the rebound of the material. As the elongation increases, the residual depth of the sample gradually decreases. The material undergoes plastic deformation after pre-stretching, resulting in an increase in its yield strength and hardness. The load-depth curve obtained by the finite element inversion is consistent with the trend of the indentation test, so the accuracy of the indentation simulation is considered to be higher.

The changes of indentation morphology with different elongations are obtained by finite element simulation. Figure 16(a) and (b) shows the indentation process of 10% elongation.

Figure 16(a) shows the loading stage of the pressing process at $t = 0.1$ s, $t = 0.3$ s, $t = 0.75$ s. It can be seen that as the pressing depth increases, the maximum principal stress of Mises gradually increases. When $t = 1.0$ s, the indenter moves up and unloads. Compared with the stress cloud diagrams at the maximum depth of the loading stage, it can be seen that the material has gone

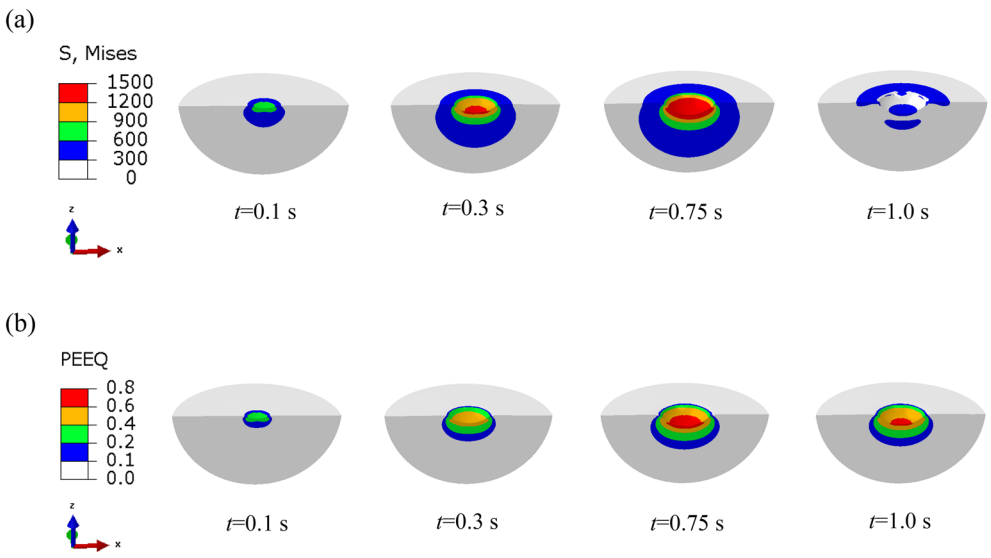

Figure 16 **(a)** Mises stress of indentation process under 10% elongation, **(b)** equivalent plastic strain (PEEQ) of indentation process under 10% elongation

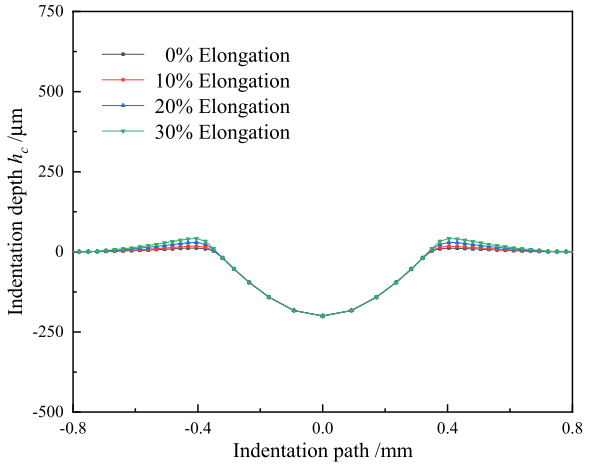

Figure 17 Comparison of maximum indentation morphology under different elongations

through the elastic recovery stage after unloading, and the maximum principal stress of Mises is reduced. Figure 16(b) shows the equivalent plastic strain (PEEQ) of the indentation process. During the loading phase, PEEQ increases as the depth of the indentation. After the indenter is pressed into the maximum indentation depth, the unloading begins. When the maximum depth is reached, the indenter starts to unload. The unloaded material passes through the elastic release stage, its strain and strain range are reduced.

The displacement increment on the same path of the material surface on the side in contact with the indenter is analyzed, as shown in Figure 17.

It can be seen from Figure 17 that the displacement increment trend of materials with different elongations on the indentation path is the same. The materials in contact with the area under the indenter will first produce elastic deformation. As the load continues to increase, the indenter will continue to press down. The material will undergo plastic deformation, and the downward increment will gradually increase. The material in the area around the indenter steadily accumulated. The maximum protrusion of undeformed material is 28.603 μm, the maximum protrusion of 10% elongation is 29.954 μm, the maximum protrusion of 20% elongation is 34.418 μm, and the maximum protrusion of 30% elongation is 39.406 μm.

5.3 Comparison of Results

The mechanical properties of materials with different elongations obtained in the indentation test need to be verified. The results obtained in the uniaxial tensile test are the agreed true values.

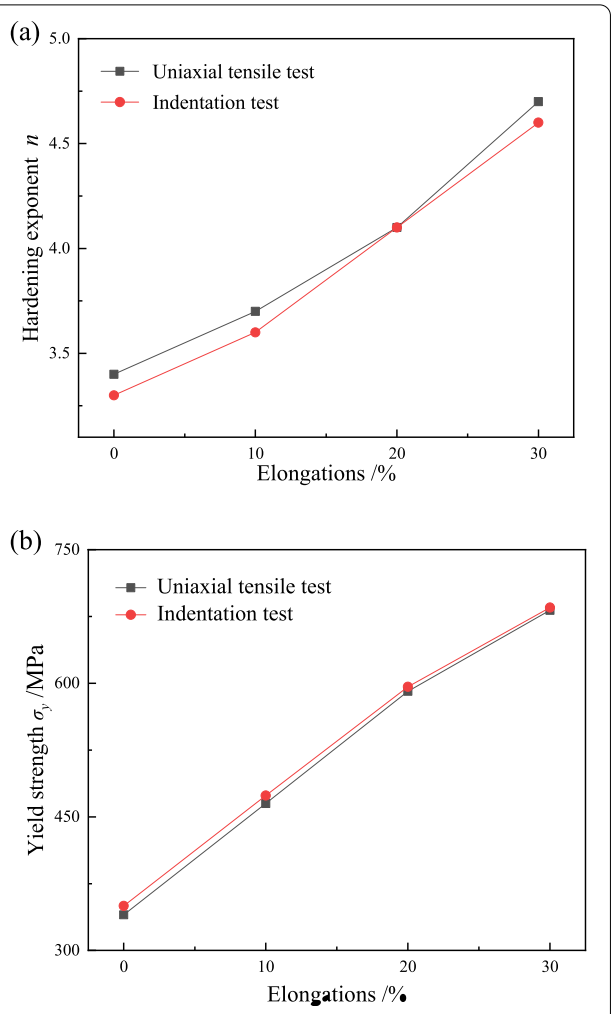

Figure 18 Comparison of mechanical parameters obtained by indentation test and tensile test under different elongations: **(a)** hardening exponent, **(b)** yield strength

Figure 18(a) and (b) shows the comparison between the mechanical properties of austenitic stainless steel 316L calculated by the indentation test and the uniaxial tensile test under the different elongation conditions.

It can be seen from Figure 18 that the mechanical property parameters of austenitic stainless steel at different elongations obtained by the indentation test are relatively close to the tensile test. The mechanical properties calculated by the indentation test have high accuracy and a small error range. The errors of the hardening exponent are less than 5%. The errors of yield strength are all less than 2.9%.

To verify the accuracy of the finite element model, it is necessary to substantiate the indentation test results obtained by the finite element method to ensure the accuracy of mechanical parameters. Figure 19 shows the

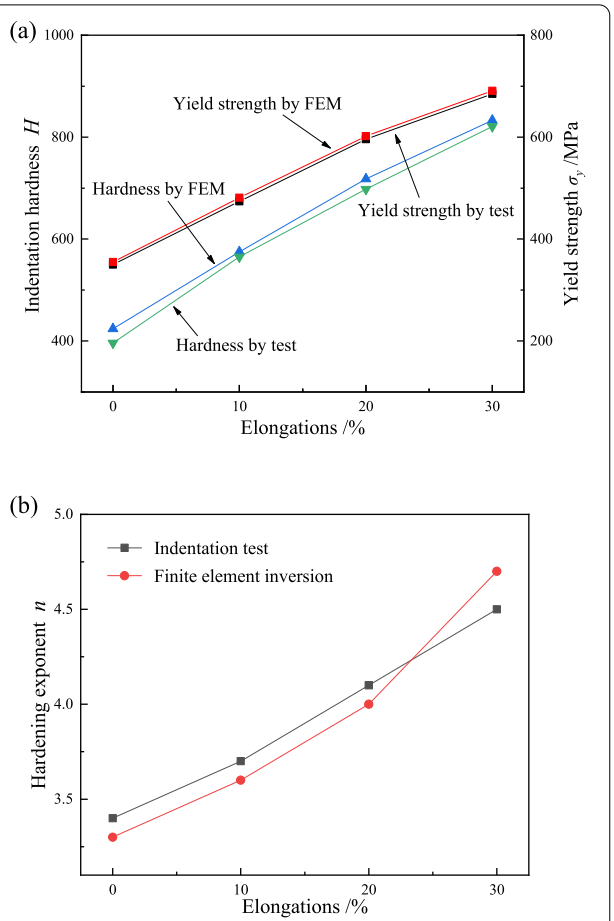

Figure 19 Comparison of mechanical parameters obtained by indentation test and finite element method with different elongations: **(a)** hardness and yield strength, **(b)** hardening exponent

comparison of the deviation of the mechanical parameters calculated from the indentation test and the finite element method.

It can be seen from Figure 19 that the mechanical properties have little difference between the indentation test and finite element simulation under different elongations. Thereby the accuracy of the established finite element model is confirmed. The errors of indentation hardness are about 5%. The errors of yield strength are below 1.5%. The errors of the hardening exponent are about 5%, and the reason for the larger error is the small transition zone between the elasticity and plasticity of the stress-strain curves, but it is within the acceptable range.

6 Conclusions

In this study, the micron-level indentation test system was built in our laboratory to perform indentation tests on austenitic stainless steel 316L under different elongations. With the aid of finite element inversion analysis, the indentation process simulation was realized, and the mechanical performance parameters of 316L were compared. The following conclusions can be drawn from this study.

(1) A suitable test program was developed for the indentation test, and the load-depth curves of austenitic stainless steel 316L under different elongations were obtained. As the elongation increases, the curves shift to the left, the resulting indentation responses become smaller, and the residual indentation depth values become smaller.
(2) The indentation test model was established by using the finite element software ABAQUS, and the relevant mechanical property parameters of materials with different elongations were obtained by inversion analysis. Comparing the finite element analysis with the indentation test, the deviations are all within 5%, which ensures the accuracy of the finite element model.
(3) Compared with the test results obtained from the tensile test based on the plate-shaped tensile sample, the deviations of the elastic-plastic material mechanical parameters, such as hardness, hardening exponent, and others are within 5% obtained through the indentation test and the finite element inversion analysis.
(4) It provides a reasonable and effective structural integrity evaluation to obtain the actual material mechanical properties of the welding and other hot or cold working areas in key structures.

Acknowledgements
No applicable.

Authors' Contributions
HX was in charge of the whole trial; JH wrote the manuscript; JZ and YX assisted with sampling and laboratory analyses. All authors read and approved the final manuscript.

Authors' Information
He Xue, born in 1961, is currently a professor at *Xi'an University of Science and Technology, China*. He received his PhD degree in 1998 from *Xi'an Jiaotong University, China*. His research interests include safety evaluation of important mechanical structures.
Jinxuan He, born in 1994, is currently a master candidate at *School of Mechanical Engineering, Xi'an University of Science and Technology, China*. His research interests include safety evaluation of important mechanical structures.
Jianlong Zhang, born in 1988, is currently an engineer at *Xi'an Special Equipment Inspection Institute, China*. He received his PhD degree from *Xi'an University of Science and Technology, China*, in 2020. Tel: +86-13679269699; E-mail: 527449153@qq.com
Yuxuan Xue, born in 1994, is currently a PhD candidate at *Department of Industrial and Manufacturing Systems Engineering, The University of Hong Kong, China*. His research interests include nanorobotics and micro-mechanics.

Funding
Supported by National Natural Science Foundation of China (Grant No. 52075434) and Key R&D Projects in Shaanxi Province (Grant No. 2021KW-36).

Competing Interests
The authors declare no competing financial interests.

Author Details
[1]School of Mechanical Engineering, Xi'an University of Science and Technology, Xi'an 710054, China. [2]Xi'an Special Equipment Inspection Institute, Xi'an 710065, China. [3]Department of Industrial and Manufacturing Systems Engineering, The University of Hong Kong, Hong Kong 999077, China.

Received: 29 December 2020 Revised: 4 September 2021 Accepted: 3 November 2021
Published online: 07 December 2021

References

[1] S Guo, E H Han, H Wang, et al. Life prediction for stress corrosion behavior of 316L stainless steel elbow of nuclear power plant. *Acta Metall Sin*, 2017, 53(4): 455–464.
[2] M D Wu, D H Xiao, W B Chen, et al. Effect of cold rolling pre-deformation on microstructure and mechanical properties of new aluminum lithium alloy. *Rare Metal Materials and Engineering*, 2020, 49(9): 3251–3259. (in Chinese)
[3] K Li, H Xue, K Zhao, et al. Determination of ratio of yield strength and reduced modulus during cold work processing in 304 austenitic stainless steel. *Key Engineering Materials,* 2019, 4784: 145–151.
[4] H Xue, K Li, S Wang, et al. Size effect analysis of hardness indentation of 316L austenitic stainless steel during cold working. *China Mechanical Engineering*, 2019, 30(1): 105–112. (in Chinese)
[5] P L Andresen. A brief history of environmental cracking in hot water. *Corrosion*, 2019, 75(3): 240–253.
[6] H Xue, Z C Zhuang, T Cao, et al. Analysis of relationship between Vickers hardness and yield stress of structural material. *Journal of Xi'an University of Science and Technology*, 2017, 37(2): 274–279. (in Chinese)
[7] F Soffel, D Eisenbarth, E Hosseini, et al. Interface strength and mechanical properties of Inconel 718 processed sequentially by casting, milling, and direct metal deposition. *Journal of Materials Processing Technology*, 2020, 291(2): 117021
[8] Y Q Li, H Xue. Micro-mechanical state at SCC tip in nuclear key structure materials. *Journal of Xi'an University of Science and Technology*, 2016, 36(3): 380–384. (in Chinese)
[9] J Lee, K Lee, S Lee, et al. Application of macro-instrumented indentation test for superficial residual stress and mechanical properties measurement for HY steel welded T-joints. *Materials*, 2021, 14(8): 2061.
[10] T Zhang, S Wang, W Wang. A study on determination of tensile properties of metals at elevated temperatures from spherical indentation tests. *The Journal of Strain Analysis for Engineering Design*, 2019, 54(5–6): 331–347.
[11] D D Zong, D Wang, W C Li, et al. Design of automatic leveling device based on marlin firmware desktop 3D printer. *Industrial Control Computer*, 2016, 29(4): 85–88.
[12] A Zhang, Z Song, C Bian. Mechanical properties of bovine cortical bone based on the automated ball indentation technique and graphics processing method. *Journal of the Mechanical Behavior of Biomedical Materials*, 2018, 78: 321.
[13] N A Stillwellwe, D Tabor. Elastic recovery of conical indentation. *Phys. Proc. Soc*, 1961, 78(2): 169–179.
[14] S I Bulychev, V P Alekhin, M K Shorshorov, et al. Determining Young's modulus from the indenter penetraion diagram. *Zavod. Lab*, 1975, 41(9): 11137–11114.
[15] F M Haggag, L J Siefken. Effects of fuel rod length on in-core relocation of liquefied material. *AIChE Symp. Ser*, 1983, 79(225): 303–309.
[16] G Das, S Ghosh, S K Sahay, et al. Influence of pre-straining on mechanical properties of HSLA steel by using ball indentation technique. *Zeitschrift Fur Metallkunde*, 2013, 95(12): 1120–1127.
[17] B Zou, Z K Wei, K S Guan. Fature toughness valuation of seel by continuous ball indentation test. *Journal of Materials Science and Engineering*, 2016, 34(4): 577–580. (in Chinese)
[18] Z K Wei, S B Wu, K S Guan. Fracture toughness of 16MnR steel evaluated by ball indentation method. *Materials for Mechanical Engineering*, 2016, 40(1): 32–34, 38. (in Chinese)
[19] U Zafar, C Hare, A Hassanpour, et al. Assessing powder flowability at low stresses using ball indentation method: Evaluation of constraint factor. *Powder Technology*, 2021, 387: 287–294.
[20] G X Zhang, W Q Wang, S Wang. Use of automated ball indentation method to evaluate the fracture toughness of Q235B steel. *Journal of Mechanical Strength*, 2018, 40(5): 1205–1208. (in Chinese)
[21] C G Su, Y Liu, W Q Wang, et al. The influence of indentation on the surface residual stress of stainless steel. *Journal of Shandong University(Engineering Science)*, 2017, 47(1): 90–96. (in Chinese)
[22] R Pamnani, V Karthik, T Jayakumar, et al. Evaluation of mechanical properties across micro alloyed HSLA steel weld joints using automated ball indentation. *Materials Science and Engineering*, 2016, 651: 214–223.
[23] K Li, H Xue, Y H Cui, et al. Establishment and validation of stress-strain constitutive equation during cold working of 304 stainless steel. *Journal of Plasticity Engineering*, 2019, 26(2): 225–232. (in Chinese)
[24] H Xue, J X He, W N Jia, et al. An approach for obtaining mechanical property of austenitic stainless steel by using continuous indentation test analysis. *Structures*, 2020, 28: 2752–2759.
[25] D L Shu. *Mechanical properties of engineering materials*. Beijing: China Machine Press, 2013. (in Chinese)
[26] T H Zhang. *Micro/Nano mechanical testing technology*. Beijing: China Machine Press, 2004. (in Chinese)
[27] G M Pharr, W C Oliver, F R Brotzen. On the generality of the relationship among contact stiffness, contact area, and elastic modulus during indentation. *Journal of Materials Research*, 1992, 7(3): 613–617.
[28] Y T Cheng, C M Cheng. Relationships between hardness, elastic modulus, and the work of indentation. *Applied Physics Letters*, 1998, 73(5): 614–616.
[29] D Tabor. The hardness and strength of metals. *Journal of the Institute of Metals*, 1951, 79(1): 1–18.
[30] J S Field, M V Swain. Determining the mechanical properties of small volumes of material from submicrometer spherical indentations. *Journal of Materials Research*, 1995, 10(1): 101–112.
[31] D Ma, T Zhang, C W Ong. Revelation of a functional dependence of the sum of two uniaxial strengths/hardness on elastic work/total work of indentation. *Journal of Materials Research*, 2006, 21(4): 895–903.